Bidirectional effect of magnetic field on electronic thermal transport of metals from all-electron first-principles calculations

Jia-Yue Yang,[1] Sheng-Ying Yue,[2] and Ming Hu[1,2,*]

[1]*Institute of Mineral Engineering, Division of Material Science and Engineering, Faculty of Georesources and Materials Engineering, RWTH Aachen University, 52064 Aachen, Germany*

[2]*Aachen Institute of Advanced Study in Computational Engineering Science (AICES), RWTH Aachen University, 52062 Aachen, Germany*

(Received 23 August 2016; revised manuscript received 8 December 2016; published 27 December 2016)

Considerable discussions have occurred about the critical role played by free electrons in the transport of heat in pure metals. In principle, any environment that can influence the dynamical behaviors of electrons would have impact on electronic thermal conductivity (κ_{el}) of metals. Over the past decades, significant progress and comprehensive understanding have been gained from theoretical, as well as experimental, investigations by taking into account the effects of various conditions, typically temperature, impurities, strain, dimensionality, interface, etc. However, the effect of external magnetic field has received less attention. In this paper, the magnetic-field dependence of electron-phonon scattering, the electron's lifetime, and κ_{el} of representative metals (Al, Ni, and Nb) are investigated within the framework of all-electron spin-density functional theory. For Al and Ni, the induced magnetization vector field and difference in electron density under external magnetic-field aggregate toward the center of unit cell, leading to the enhanced electron-phonon scattering, the damped electron's lifetime, and thus the reduced κ_{el}. On the contrary, for Nb with strong intrinsic electron-phonon interaction, the electron's lifetime and κ_{el} slightly increase as external magnetic field is enhanced. This is mainly attributed to the separately distributed magnetization vector field and difference in electron density along the corner of unit cell. This paper sheds light on the origin of influence of external magnetic field on κ_{el} for pure metals and offers a new route for robust manipulation of electronic thermal transport via applying external magnetic field.

DOI: 10.1103/PhysRevB.94.235153

I. INTRODUCTION

Thermal conductivity, one of the fundamentally physical properties, measures a material's capability to conduct heat and specifies its enormous applications [1,2]. Electrons and phonons are the two well-known heat carriers in solids [3]. In semiconductors and insulators, phonons dominate heat transport, and the microscopic process can be effectively described by the Peierls-Boltzmann transport equation (BTE) within the framework of density functional theory (DFT) [4–6]. Electrons influence phonon thermal transport mainly via electron-phonon interaction (EPI) at intermediate and higher temperatures [7,8]. In metals consisting of free electrons, the thermal transport is dominated by electrons, and phonons influence electronic thermal transport mainly via EPI [9].

Study on the contribution of magnons (spin wave), the third elemental excitation, to thermal transport has long received extraordinary attention [10,11]. With the development of spin DFT [12–15], the noncollinear magnetism is described, and physical properties modulated by external magnetic field ($\boldsymbol{B}_{ext}$) can be theoretically simulated by first principles. Recently, Jin *et al.* [16] demonstrated that $\boldsymbol{B}_{ext}$ could alter the anharmonicity of interatomic bonds in diamagnetic semiconductor InSb and thus modulate phonon transport process. Among various ways to engineer thermal transport [5,17,18], the magnetic field demonstrates great advantage with the merit of being controllable, nondestructive, and easy-to-apply [19]. Yet, the key scientific challenge is to better understand how thermal transport of electrons and phonons are modulated under $\boldsymbol{B}_{ext}$. Though previous literatures [20–23] studied the effect of $\boldsymbol{B}_{ext}$ on thermal conductivity of materials, such as metals and superconductor films, via theoretical simulations as well as experimental measurements, the underlying mechanism still remains unrevealed.

In this paper, the electronic thermal transport in metals (Al, Ni, and Nb) modulated by $\boldsymbol{B}_{ext}$ is investigated within the framework of spin DFT. The metals were chosen as model systems mainly because electrons dominate the thermal transport, and lattice contribution (phonons) can be negligible [9]. The modulated electronic thermal transport in metals is studied mainly by computing the electron-phonon scattering under the influence of $\boldsymbol{B}_{ext}$. Then, the key parameter of the electron's lifetime is extracted and transferred to compute electronic thermal conductivity (κ_{el}) based on the Boltzmann transport theory.

II. COMPUTATIONAL METHODOLOGY

In the presence of $\boldsymbol{B}_{ext} = \nabla \times \boldsymbol{A}_{ext}$, the Kohn-Sham equation describes the noninteracting electrons states as [14]

$$(-1/2\nabla^2 + v_s + \mu_B \boldsymbol{\sigma} \cdot \boldsymbol{B}_s)\Phi_i(r) = \varepsilon_i \Phi_i(r) \qquad (1)$$

and can be derived by minimizing the total energy within the framework of spin DFT. Based on the two-component Pauli spinors Φ_i, the noncollinear electron density $\rho(\mathbf{r}) = \sum_i^{occ} \Phi_i^\dagger(\mathbf{r})\Phi_i(\mathbf{r})$ and magnetization density $\mathbf{m}(\mathbf{r}) = \mu_B \sum_i^{occ} \Phi_i^\dagger(\mathbf{r})\sigma\Phi_i(\mathbf{r})$ are calculated to describe the total energy $E[\rho, \boldsymbol{m}]$ [14]

$$E[\rho,\mathbf{m}] = T_s[\rho,\mathbf{m}] + V_{ext}[\rho] + \boldsymbol{B}_{ext} \cdot \mathbf{m} + U[\rho] + E_{XC}[\rho,\mathbf{m}], \qquad (2)$$

*Author to whom all correspondence should be addressed: hum@ghi.rwth-aachen.de

where T_s, V_{ext}, and U are the kinetic energy, external potential, and Hartree energy, respectively, $\boldsymbol{\sigma}$ is the vector of Pauli matrices, and μ_B is magnetic permeability. In Eq. (1), the effective scalar potential $v_s = v_{\text{ext}} + v_H + v_{\text{XC}} + 1/2c^2 A_{\text{ext}}^2$ and magnetic vector field $\boldsymbol{B}_s = \boldsymbol{B}_{\text{ext}} + \boldsymbol{B}_{\text{XC}}$ are constructed with the exchange-correlation (XC) potential v_{XC} and XC magnetic field $\boldsymbol{B}_{\text{XC}}$, respectively, as $v_{\text{XC}} = \partial E_{\text{XC}}[\rho,\mathbf{m}]/\partial\rho$ and $\boldsymbol{B}_{\text{XC}} = \partial E_{\text{XC}}[\rho,\mathbf{m}]/\partial\mathbf{m}$. The exact functional form of E_{XC} cannot be computed, and some approximations have to be made in practice. To ensure the numerical analysis as accurately as possible, the exact-exchange-only approximation was adopted, and the augmented plane wave basis was chosen to avoid shape approximations for the effective potential [14]. To solve the above Kohn-Sham equations, the two-step variational process was followed. (1) At the first variational step, the Hamiltonian containing only the scalar potential v_s is solved, and the scale states serve as the basis for the second step. (2) At the second variational step, the magnetic terms and spin-orbital coupling are included [14,16]. By solving the Kohn-Sham equations, the two-component spinors (Φ), noncollinear density (ρ), and magnetization density ($\boldsymbol{m}$) under $\boldsymbol{B}_{\text{ext}}$ can be obtained and further applied to compute relevantly physical quantities.

To investigate the magnetic-field dependent electronic thermal transport, the key lies in computing the influence of external magnetic field on the intrinsic EPI. The EPI fundamentally arises from the coupling of Bloch states with lattice vibration, and such process can be described by averaging Eliashberg spectral function ($\alpha^2 F$) around the Fermi surface (E_F) [24] as

$$\alpha^2 F(\omega) = 1/N_{E_F} \sum_{\mathbf{k},\mathbf{k}+\mathbf{q}} \times \sum_{v} |g_{\mathbf{k},\mathbf{k}+\mathbf{q},v}|^2 \delta(\varepsilon_{\mathbf{k}})\delta(\varepsilon_{\mathbf{k}+\mathbf{q}})\delta(\omega - \omega_{\mathbf{q}v}). \quad (3)$$

The sum is taken over the initial and final Bloch state $\boldsymbol{k}$ and $\boldsymbol{k}+\boldsymbol{q}$ and phonon branch v and then averaged by the number of energy states N around the Fermi level. The $g_{\boldsymbol{k},\boldsymbol{k}+\boldsymbol{q},v}$ is the EPI matrix, and the δ function ensures the energy conversation during the electron-phonon scattering process. Then, the averaged electron-phonon coupling strength (λ) can be computed as $2\int \alpha^2 F(\omega)/\omega d\omega$, and the induced electron's linewidth (Γ) is expressed as [24]

$$\Gamma(\varepsilon) = 2\pi \int_0^{\omega_{\max}} \alpha^2 F(\omega_{\mathbf{q}v})[1 - f(\varepsilon - \omega_{\mathbf{q}v}) + f(\varepsilon + \omega_{\mathbf{q}v}) + 2n(\omega_{\mathbf{q}v})]d\omega_{\mathbf{q}v}, \quad (4)$$

where electrons obey the Fermi-Dirac distribution (f) and phonons follow the Bose-Einstein distribution (n). The average electron's lifetime (τ) can be extracted as $\hbar/\Gamma$ and then used to compute electronic transport properties. Based on the free gas model, the conductivity tensor ($\sigma_{\alpha\beta}$) is written as $\sigma_{\alpha\beta} = e^2\tau u_\alpha u_\beta$, where u is the group velocity. By projecting the $\boldsymbol{k}$-space tensor $\sigma_{\alpha\beta}$ into the energy range, one can effectively compute κ_{el} as [25] (see Sec. S1 in the Supplemental Material [26])

$$\kappa_{el} = 1/(e^2 T\Omega) \int \sigma_{\alpha\beta}(\varepsilon)(\varepsilon - \mu)^2[-\partial f_\mu(T;\varepsilon)/\partial\varepsilon]d\varepsilon, \quad (5)$$

where μ is the chemical potential, Ω is the volume, and $\sigma_{\alpha\beta}(\varepsilon)$ is the energy projected conductivity tensors.

The inclusion of $\boldsymbol{B}_{\text{ext}}$ is implemented by the state-of-the-art all-electron full-potential linearized augmented plane wave (FP-LAPW) code ELK [14,27]. With the augmented plane wave basis, it can be used to accurately compute the effective potential under external magnetic field without local discontinuities in the XC potentials introduced by functional approximations [13]. To compute the EPI in Al, Ni, and Nb, the primitive cell containing one atom was used, and the external magnetic field was applied in the [001] direction. The converged results were obtained by performing simulations with $32\times32\times32$ k-point mesh, $4\times4\times4$ q-point mesh, and eight empty states. After the EPI calculations, the electron's lifetime was extracted and further applied to compute electronic transport properties. Such procedure was accomplished by Quantum Espresso [28] and BoltzTrap [25] packages. By computing electronic energy states and the electron's lifetime of metals, the electronic transport properties, e.g., κ_{el} and σ, can be obtained.

III. RESULTS AND DISCUSSIONS

Under the influence of $\boldsymbol{B}_{\text{ext}}$, microscopic electrons are subjected to an external Lorentz force, and the distribution of electron density perturbs. The local magnetization vector field emerges, and its magnetic moment is verified to be linear with $\boldsymbol{B}_{\text{ext}}$. By comparing the distribution of $\boldsymbol{m}$ and change in electron density ($\Delta\rho$) in the presence of $\boldsymbol{B}_{\text{ext}}$, the opposite distribution pattern is observed for Al, Ni, and Nb. In Fig. 1, the modulus of induced $\boldsymbol{m}$ and $\Delta\rho$ under external magnetic field projected along [001] direction for Al, Ni, and Nb, respectively, is presented. Its absolute value can help determine the distribution pattern of the induced magnetization vector field plane in metals. Due to the noncollinearity, the induced $\boldsymbol{m}$ and $\Delta\rho$ along other directions also exist, but their absolute value is small. Under the action of external Lorentz force, the quantum behaviors of electrons are influenced by external magnetic field. It shows that under the influence of $\boldsymbol{B}_{\text{ext}}$, the modulus of the induced $\boldsymbol{m}$ concentrates towards the center of unit cell in Al and Ni, which is in positive correlation with the distribution pattern of $\Delta\rho$. It means that the large modulus of the induced $\boldsymbol{m}$ corresponds to big electron density difference. For Nb, however, $\boldsymbol{m}$ is symmetrically separate along the corner of the unit cell, and its value is negatively correlated with $\Delta\rho$. The difference in the distribution pattern of the modulus of the induced $\boldsymbol{m}$ and $\Delta\rho$ can intrinsically interpret the variation for the change trend of electronic thermal conductivity in Al, Ni, and Nb.

To interpret it from the atomic level, the electron localization function (ELF) for Al, Ni, and Nb is calculated. In Figs. 2(a) and 2(b), we observe that there exists relatively low localization and many itinerant electrons in Al and Ni. Consequently, free electrons are easily subjected to the Lorentz force in the presence of an external magnetic field and aggregate towards the center of the unit cell, leading to the increased electron-phonon coupling strength and decreased electron's lifetime in Al and Ni. Under the influence of $\boldsymbol{B}_{\text{ext}}$, the delocalized electrons tend to aggregate towards the center of the unit cell. For Nb, electrons are highly localized around core

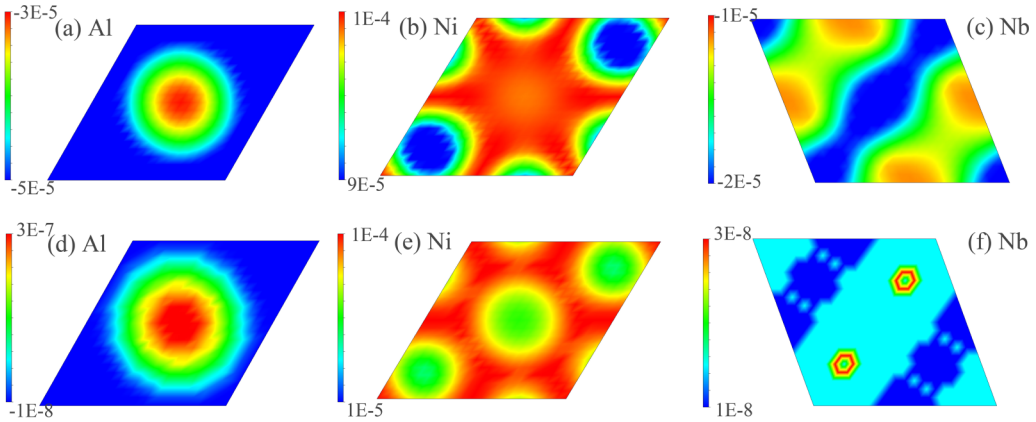

FIG. 1. The 2D slice projected along the [001] direction of (a)–(c) the modulus of induced magnetization vector field under external magnetic field $\boldsymbol{B}_{\text{ext}} = 0.1$ a.u. and (d) –(f) the induced difference in electron density under $\boldsymbol{B}_{\text{ext}} = 0.01$ a.u. and 0.1 a.u. for Al, Ni, and Nb, respectively.

ions. As a consequence, relatively fewer itinerant electrons exist in Nb, and the induced $\Delta\rho$ by external Lorentz force tends to separately distribute along the core ions in the corner of unit cell, leading to the damped electron-phonon coupling strength. Besides, due to the highly localized electrons, the modulus of induced $\boldsymbol{m}$ symmetrically distributes along the corner of unit cell, and its value is negatively correlated with $\Delta\rho$. The different behavior of the electron localization in Al, Ni, and Nb is of great importance to explain the difference in the absolute value of κ_{el}.

The induced $\Delta\rho$ under $\boldsymbol{B}_{\text{ext}}$ greatly influences the electron-phonon scattering in metals. For Al and Ni with $\Delta\rho$ concentrating towards the center of unit cell, the average α^2F increases as the magnetic field is enhanced (see Sec. S2 in the Supplemental Material [26]), indicating the enhanced EPI. Besides, it observes that the dominant peak of α^2F locates at 37.67 meV and 30.81 meV for Al and Ni, respectively, corresponding to the highest acoustic phonon branch. For Nb, the dominant peak of α^2F locates at 16.26 meV, where the phonon density of states aggregates. Moreover, as the strength of $\boldsymbol{B}_{\text{ext}}$ increases, the dominant peak of α^2F is slightly reduced, and the EPI is damped. To interpret this, the influence of $\boldsymbol{B}_{\text{ext}}$ on quantum behaviors of electrons and phonons is investigated. Upon comparing the phonon dispersion and phonon density of states in the presence of varying $\boldsymbol{B}_{\text{ext}}$, it shows that there exists little change for Al, Ni, and Nb, which suggests that the effect of external magnetic field on electronic thermal transport in metals occurs mainly via influencing the quantum behaviors of electrons but not phonons. Furthermore, the difference in the modified distribution of electrons of Al, Ni, and Nb leads to the enhanced or damped EPI. For Al and Ni, the concentrated electrons towards the center of unit cell enhance the EPI, while the separately distributed $\Delta\rho$ in the corner of unit cell of Nb damps the EPI.

With the magnetic-field dependent average α^2F, the related λ and τ for Al, Ni, and Nb at room temperature can be effectively computed. In this paper, the external magnetic field over the range 0.001–0.30 a.u. (1 a.u. = 1715.26 Tesla) is applied. On the one hand, the choice of the small magnetic field, such as 0.001–0.01 a.u. (∼1.7–17 Tesla), can enable experimentalists to verify the theoretical simulations. On the other hand, the use of very large magnetic fields, such as 0.01–0.3 a.u. (∼17–510 Tesla), may help elucidate physical mechanisms that may be obscured at smaller magnetic fields and prompt future experimental and theoretical work [15]. The theoretically predicted λ in the absence of $\boldsymbol{B}_{\text{ext}}$ is 0.44, slightly smaller than the value of 0.49 [9] but in good agreement with measured data of 0.38–0.48 [29]. In Fig. 3(a), it shows that the calculated λ for Al slightly increases for $\boldsymbol{B}_{\text{ext}}$ up to 0.02 a.u. and then keeps almost constant for stronger magnetic field. For Ni, the calculated λ slightly increases as external magnetic field is enhanced. For instance, the λ is 0.2321 at $\boldsymbol{B}_{\text{ext}} = 0.001$ a.u., and it gradually increases to 0.2523 at $\boldsymbol{B}_{\text{ext}} = 0.3$ a.u. However, the opposite trend is observed for Nb, where λ slightly reduces with increasing $\boldsymbol{B}_{\text{ext}}$. In Fig. 3(b), it is observed that the calculated τ of Nb slightly increases as $\boldsymbol{B}_{\text{ext}}$ is enhanced, which is consistent with the change trend of the reduced λ. For Al and Ni, the trend is opposite, and the computed τ decreases by applying stronger $\boldsymbol{B}_{\text{ext}}$. It is worth pointing out an interesting phenomenon that

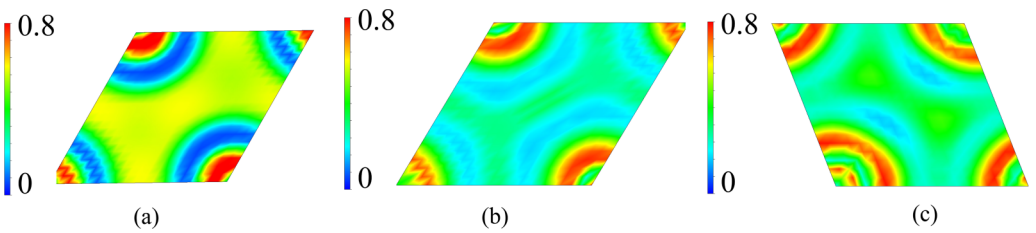

FIG. 2. The 2D electron localization function (ELF) of (a) Al, (b) Ni, and (c) Nb projected along the [001] direction (the same direction as the applied magnetic field).

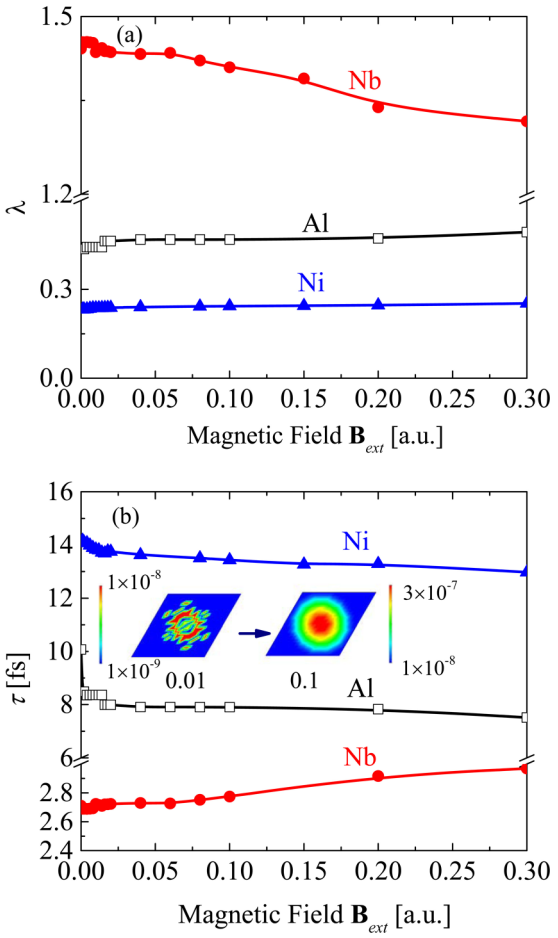

FIG. 3. Magnetic-field dependent (a) electron-phonon coupling strength (λ) and (b) the electron's lifetime (τ) averaged over the Fermi surface for Al, Ni, and Nb at 300 K. The spline lines are guide for eyes. (Inset) Comparison of the induced $\Delta\rho$ in Al under the external magnetic field of 0.01 a.u. and 0.1 a.u. with the case of $\boldsymbol{B}_{\rm ext} = 0$ a.u. (see text for details).

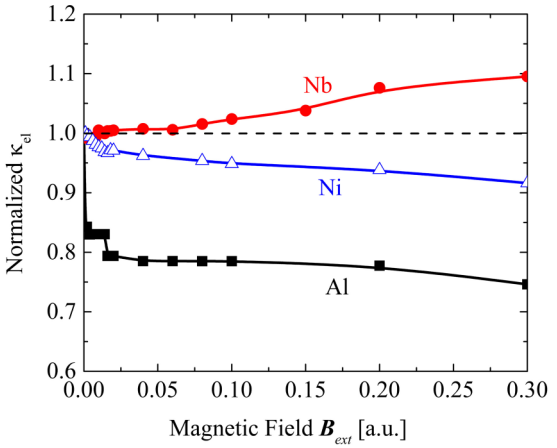

FIG. 4. Magnetic-field dependent electronic thermal conductivity of Al, Ni, and Nb at 300 K. The thermal conductivity results are normalized by their respective value in the absence of external magnetic field. The spline lines are guide for eyes.

there exists a sharp reduction in τ of Al for $\boldsymbol{B}_{\rm ext}$ up to 0.01 a.u. To interpret this, the calculated electron densities of Al under $\boldsymbol{B}_{\rm ext} = 0$, 0.01, and 0.1 a.u. are compared. It shows that there exists relatively large $\Delta\rho$ in the presence of the external magnetic field (0.01 a.u.), with the largest amplitude of 10^{-8} a.u.$^{-3}$ (1 a.u. = 0.529177 Å). Furthermore, the induced $\Delta\rho$ exhibits approximately the shape of circle, with the large values concentrating towards the center. When the $\boldsymbol{B}_{\rm ext}$ is enhanced further to 0.1 a.u., the absolute value of the induced $\Delta\rho$ enlarges to 3×10^{-7} a.u.$^{-3}$, and the shape of circle becomes clear, as shown in Fig. 3(b). It concludes that the concentrating $\Delta\rho$ towards the center induces the continuous decrease in τ and that such change then becomes slight after $\Delta\rho$ reaching to the saturated shape.

After explicitly obtaining electron's lifetime by first principles, the $\kappa_{\rm el}$ can be predicted without empirical parameters. In Fig. 4, the theoretically predicted magnetic-field dependent $\kappa_{\rm el}$ for Al, Ni, and Nb at 300 K are presented. Here, for comparison, the $\kappa_{\rm el}$ is normalized by their respective value without $\boldsymbol{B}_{\rm ext}$. In the absence of $\boldsymbol{B}_{\rm ext}$, the $\kappa_{\rm el}$ of Al is calculated to be 232.73 W/mK at 300 K, which is relatively smaller than literature data of 246 W/mK [9] but larger than the calculated value of 223.93 W/mK using direct nonequilibrium first-principles molecular dynamics [30]. By solving the BTE using first-principles calculations [6], the predicted lattice thermal conductivity of Al at 300 K is 7.91 W/mK, and the total thermal conductivity is 240.64 W/mK, which agrees well with the experimental value of 237 W/mK [31]. For Ni, the predicted $\kappa_{\rm el}$ in the presence of magnetic field (0.001 a.u.) is 92.14 W/mK and is consistent with the value of 90.7 W/mK [32]. The reason to start with $\boldsymbol{B}_{\rm ext}$ of 0.001 a.u. for Ni is that slight imaginary phonon frequencies exist in Ni in the presence of an external magnetic field, with the present supercell approach to include an external magnetic field into computing phonon dispersion curve. However, for Nb, the predicted $\kappa_{\rm el}$ is 36.9 W/mK and is relatively smaller than the literature value of 54 W/mK [33]. The plausible explanation is that the theoretically calculated electron-phonon coupling strength of 1.44 is relatively larger than the literature value of 1.24 [34], resulting in the reduced τ and $\kappa_{\rm el}$. Apart from that, we find bidirectional magnetic-field effect on the electronic thermal transport in the three metals studied: the theoretically predicted $\kappa_{\rm el}$ of Nb is increased by 12% with the magnetic field increasing to 0.3 a.u., while for Al and Ni the calculated $\kappa_{\rm el}$ is decreased by 5% and 25%, respectively, with increasing magnetic field. For Al, a relatively sharp reduction at $\boldsymbol{B}_{\rm ext} = 0.001$ a.u. exists, corresponding to the steep decrease in electrons' lifetime, as shown in Fig. 3(b). The difference in the change trend between Al, Ni, and Nb is intrinsically related to their electron localization. It is shown in Fig. 2 that the electron localization of Al is the smallest, indicating that the most itinerant electrons in Al exist. Under the action of Lorentz force induced by an external magnetic field, the itinerant electrons tend to move in metals. For Al and Ni, the induced $\Delta\rho$ aggregate towards the center of unit cell and thus results in the enhanced EPI and reduced $\kappa_{\rm el}$. Consequently, the difference in the amplitude of decreased $\kappa_{\rm el}$ under external magnetic field in Al and Ni is mainly caused by the variation in the number of itinerant electrons. However, for Nb, the change trend in $\kappa_{\rm el}$ is opposite, and the root reason

is that strong electron localization occurs and that electrons are mainly localized around Nb atoms. As a consequence, the $\Delta\rho$ is distributed along the corner of unit cell under a strong external magnetic field and thus induces the damped EPI and increased κ_{el}.

Besides κ_{el}, the electrical conductivity (σ) of those metals can also be obtained by first principles. In Fig. S6 of the Supplemental Material [26], the electrical conductivity σ for Al, Ni, and Nb at 300 K is presented. In the absence of an external magnetic field, the theoretically predicted σ of Al, Ni, and Nb is 3.2×10^7 S/m, 1.2×10^7 S/m, and 5.1×10^6 S/m, respectively, and is consistent with the reference data of 3.8×10^7 S/m, 1.4×10^7 S/m, and 6.7×10^6 S/m [35]. Moreover, as the external magnetic field is enhanced, the change trend of σ is the same as that of κ_{el} in Al, Ni, and Nb (see Fig. S7 in the Supplemental Material [26]). In Al, for instance, a sharp decrease occurs at $\boldsymbol{B}_{ext} = 0.001$ a.u., and then σ slight changes with increasing magnetic field. Theoretically, σ and κ_{el} have the same change trend with the external magnetic field, and, consequently, the ratio between them stays constant, which obeys the Wiedemann–Franz law [31]. Following the Wiedemann–Franz law, the calculated Lorentz number (defined as $L = \kappa_{el}/\sigma T$) for Al, Ni, and Nb is 2.42×10^{-8} W/ΩK^2, 2.41×10^{-8} W/ΩK^2, and 2.47×10^{-8} W/ΩK^2, respectively, which is consistent with the constant of 2.44×10^{-8} W/ΩK^2.

IV. CONCLUSION

In summary, the influence of an external magnetic field on the electron's lifetime and electronic thermal transport in three representative metals (Al, Ni, and Nb) is investigated by considering intrinsic electron-phonon scattering from the all-electron first-principles calculations. Upon applying the external magnetic field, the magnetization vector field is induced, and the difference in electron density demonstrates distinct distribution pattern for Al, Ni, and Nb, resulting in the opposite trend in the magnetic-field dependent electron-phonon scattering, the electrons' lifetime, and electronic thermal conductivity. For Al and Ni, the predicted electronic thermal conductivity decreases as external magnetic field increases. This is mainly caused by the aggregated electron density towards the center of the unit cell, which enhances the EPI and thus suppresses the electron's lifetime. For Nb, the electron density is separately distributed along the corner of the unit cell under strong external magnetic field, which leads to the reduced electron-phonon scattering and thus enhanced electronic thermal conductivity. By elucidating this process, the computational framework presented herein can be straightforwardly extended to heavily doped semiconductors or metallic systems where electrons dominate heat transport. The ability to alter the electronic thermal transport by external magnetic field also provides guidance for the vast amount of applications with tailored electronic thermal conductivity. We expect that our study will stimulate future experiments to manipulate thermal conductivity of pure metals without altering its original structures with such process being reversible. This is fundamentally different from the conventional strategy in literature, where irreversible structure modification is usually involved, such as alloying, doping, low dimensionality, and nanostructuring.

ACKNOWLEDGMENT

The authors gratefully acknowledge the computing time granted by the John von Neumann Institute for Computing (NIC) and provided on the supercomputer JURECA at Forschungszentrum Jülich, Germany (Project ID: JHPC37).

[1] D. A. Broido, M. Malorny, G. Birner, N. Mingo, and D. A. Stewart, Appl. Phys. Lett. **91**, 231922 (2007).
[2] L. Lindsay, D. A. Broido, and T. L. Reinecke, Phys. Rev. B **87**, 165201 (2013).
[3] J. M. Ziman, *Electrons and Phonons: The Theory of Transport Phenomena in Solids* (Oxford University Press, New York, 1960).
[4] K. Esfarjani, G. Chen, and H. T. Stokes, Phys. Rev. B **84**, 085204 (2011).
[5] J. Garg, N. Bonini, B. Kozinsky, and N. Marzari, Phys. Rev. Lett. **106**, 045901 (2011).
[6] W. Li, J. Carrete, N. A. Katcho, and N. Mingo, Comput. Phys. Commun. **185**, 1747 (2014).
[7] L. J. Sham and J. M. Ziman, Solid State Phys. **15**, 221 (1963).
[8] B. Liao, B. Qiu, J. Zhou, S. Huberman, K. Esfarjani, and G. Chen, Phys. Rev. Lett. **114**, 115901 (2015).
[9] A. Jain and A. J. H. McGaughey, Phys. Rev. B **93**, 081206 (2016).
[10] D. J. Sanders and D. Walton, Phys. Rev. B **15**, 1489 (1977).
[11] C. Hess, C. Baumann, U. Ammerahl, B. Büchner, F. Heidrich-Meisner, W. Brenig, and A. Revcolevschi, Phys. Rev. B **64**, 184305 (2001).
[12] G. Vignale and M. Rasolt, Phys. Rev. B **37**, 10685 (1988).
[13] S. Sharma, S. Pittalis, S. Kurth, S. Shallcross, J. K. Dewhurst, and E. K. U. Gross, Phys. Rev. B **76**, 100401 (2007).
[14] S. Sharma, J. K. Dewhurst, C. Ambrosch-Draxl, S. Kurth, N. Helbig, S. Pittalis, S. Shallcross, L. Nordström, and E. K. U. Gross, Phys. Rev. Lett. **98**, 196405 (2007).
[15] S. Rohra and A. Görling, Phys. Rev. Lett. **97**, 013005 (2006).
[16] H. Jin, O. D. Restrepo, N. Antolin, S. R. Boona, W. Windl, R. C. Myers, and J. P. Heremans, Nat. Mater. **14**, 601 (2015).
[17] M. Hu, K. P. Giapis, J. V. Goicochea, X. Zhang, and D. Poulikakos, Nano Lett. **11**, 618 (2011).
[18] M. Hu and D. Poulikakos, Nano Lett. **12**, 5487 (2012).
[19] H. E. Knoepfel, *Magnetic Fields: A Comprehensive Theoretical Treatise for Practical Use* (Wiley, New York, 2008).
[20] D. E. Morris and M. Tinkham, Phys. Rev. **134**, A1154 (1964).
[21] H. M. Brown, Phys. Rev. **32**, 508 (1928).
[22] B. Yuya, I. Takamitsu, S. Ken-ichi, K. Hidekazu, F. Hiroyuki, K. Masaki, and T. Takao, Meas. Sci. Tech. **23**, 045103 (2012).
[23] A. Fevrier and D. Morize, Cryogenics **13**, 603 (1973).
[24] P. B. Allen and B. Mitrović, Solid State Phys. **37**, 1 (1983).
[25] G. K. H. Madsen and D. J. Singh, Comput. Phys. Commun. **175**, 67 (2006).

[26] See Supplemental Material at http://link.aps.org/supplemental/10.1103/PhysRevB.94.235153 for details on the computational methodology, magnetic-field dependent phonon dispersion curve and electron-phonon scattering, electronic thermal conductivity, and electrical conductivity.

[27] J. K. Dewhurst, S. Sharma, L. Nordström, F. Cricchio, O. Grånäs, H. Gross, C. Ambrosch-Draxl, C. Persson, F. Bultmark, C. Brouder, R. Armiento, A. Chizmeshya, P. Anderson, I. Nekrasov, F. Wagner, F. Kalarasse, J. Spitaler, S. Pittalis, N. Lathiotakis, T. Burnus *et al.*, ELK FP-LAPW code, version 3.3.17 (2016), http://elk.sourceforge.net.

[28] P. Giannozzi, S. Baroni, N. Bonini, M. Calandra, R. Car, C. Cavazzoni, D. Ceresoli, G. L. Chiarotti, M. Cococcioni, I. Dabo, A. D. Corso, S. de Gironcoli, S. Fabris, G. Fratesi, R. Gebauer, U. Gerstmann, C. Gougoussis, A. Kokalj, M. Lazzeri, L. Martin-Samos *et al.*, J. Phys.: Condens. Matter **21**, 395502 (2009).

[29] G. Grimvall, Phys. Scr. **14**, 63 (1976).

[30] S. Y. Yue, X. Zhang, S. Stackhouse, G. Qin, E. Di Napoli, and M. Hu, Phys. Rev. B **94**, 075149 (2016).

[31] C. Kittel, *Introduction to Solid State Physics*, 6th ed. (Wiley, New York, 1986).

[32] R. W. Powell, R. P. Tye, and M. J. Hickman, Inter. J. Heat Mass Transf. **8**, 679 (1965).

[33] F. Koechlin and B. Bonin, Supercond. Sci. Technol. **9**, 453 (1996).

[34] B. N. Harmon and S. K. Sinha, Phys. Rev. B **16**, 3919 (1977).

[35] P. L. Rossiter, *The Electrical Resistivity of Metals and Alloys* (Cambridge University Press, New York, 1987).